Publication No. WI-2021-03

01 June 2021

The Watershed Institute

Applied Environmental Science
California State University
Monterey Bay

100 Campus Center, Seaside, CA
93955-8001

CCoWS Central Coast Watershed Studies

Post-fire Debris Flows in the Carmel Watershed: Assessing USGS Predictions and Impacts on Steelhead Spawning Gravel

CSUMB GEOL 460 Class:

Joseph Randolph (co-editor)
Alyssa French (co-editor)
Colin Bergman
Devon Campbell
Rebecca Munster
Charlotte Obiedzenski
Gabriel Quintana
Andi Susantio
Skylar Wolfe
Mattole Whitaker
Conor Zumbach
Dr. Doug Smith (instructor)

Contact:

dosmith@csumb.edu

Student authors listed alphabetically after coeditors

Acknowledgements

We would like the thank Jamie Schnieders and Lauren Marshall for their fieldwork, California American Water for access to our study site, the Monterey Peninsula Water Management District for their collaboration. We gratefully acknowledge CSU COAST and the USGS geological hazards science center for their partial funding of this study.

Disclaimer:

This report primarily represents student work completed within the constraints of a semester-long, limited-verification college class setting.

This report may be cited as:

CSUMB Class GEOL 460: Randolph J., French A., Bergman C., Campbell, D., Munster, R., Obiedzenski, C., Quintana G., Susantio A., Wolfe S., Whitaker M., Zumbach C. and Smith D. 2021. Post-fire Debris Flows in the Carmel Watershed: Assessing USGS Predictions and Impacts on Steelhead Spawning Gravel. Watershed Institute, California State University Monterey Bay, Publication No. WI-2021-03, 38pp.

Executive Summary

Post-wildfire debris flows have been known to cause extensive property damage and claim lives. Extensive debris flows are known to occur in post-wildfire areas that are exposed to high intensity rain. Due to urban expansion into areas that could experience slope hazards a method of post-fire debris flow hazard prediction is increasingly valuable. The USGS has refined statistical models to both determine probability of debris flows and estimate volumes of potential debris flows deposits for recently burned slopes areas. This study focused on nine basins in the Carmel River Watershed that were burned in the 2020 Carmel Fire. After a high intensity rain event on January 27, 2021, debris flows occured and measurements of the flow deposits were captured. Debris flow occurrences and volumes were compared to those predicted by the USGS model. The USGS probability model was found to have accurately predicted debris flow probability. Observed debris flow volume estimates were less than those predicted by the USGS models; however, this may have been due to the erosion of deposited material during high flow in the Carmel River. The second objective of our study was an evaluation of debris flow deposits for appropriately sized Steelhead trout spawning gravel. Our study determined that although spawning gravel was present in the debris flows, an insignificant amount was deposited in the river.

Table of Contents

1 Introduction

Post-wildfire related slope failures in the form of landslides and debris flows are well known to cause extensive property damage and loss of life globally. Every year, hundreds of lives are lost and millions of dollars of property damage occur due to dangerous debris flows. Costa (1984) cites an annual death toll of 90 lives per year due to debris flows. In 1970, a massive debris flow triggered an earthquake claiming an estimated 17,000 lives in Peru (Costa 1984). Risk associated with slope failures increases as urban development extends to foothills and mountainous areas (Staley et al. 2016).

Debris flows are rapid, gravity-induced slope failures that are triggered by excess moisture (Costa 1984). Post-wildfire effects on land cover in combination with high volume precipitation events can cause catastrophic slope failure. The probability of slope failure is drastically increased when basin slope vegetation is exposed to high intensity burns during wildfire events (Staley et al. 2016). The roots that once anchored a soil mass in place may not be effective after exposure to high intensity burns when moisture levels are exacerbated by extreme precipitation events. Additional moisture contributes to an increase in soil mass; without vegetative root systems adding stability to soil masses, the probability of debris flows is greatly increased (Cannon et al. 2000).

Two distinct types of debris flow processes that are specifically related to post-fire basin slope exposure have been distinguished. One type of flow is infiltration-triggered soil slip, which occurs when a landmass becomes mobile as a fluid debris flow due to heavy precipitation (Cannon 2000). This type of flow leaves a distinct scar in the landscape where the mass is released from the slope. The second type of debris flow is runoff-dominated sediment erosion which is caused by intense runoff events. This type of debris flow initiation can originate from a lack of soil infiltration due to intense burns (Cannon et al. 2000). Such runoff contributes to rilling, channel incising, and gullying which deposits loose material into slope channels where it accumulates until precipitation-induced mobilization (Cannon et al. 2000).

Wildfire related hazards in the western United States have become more prevalent in recent years. Due to increasing wildfire events as well as expanding urban development in areas predisposed to basin slope wildfires (Westerling et al. 2006). A method used to predict slope failure would be inherently valuable to protect urbanized areas from the dangers of mass wasting

processes. This method utilized known variables such as: burn severity, soil properties, basin morphology, and precipitation conditions as parameters in a linear model that estimates the volumes of debris upon slope failure. Logistic regression of variables of a particular basin could be entered into the linear model to estimate the probability of slope failure based upon required inputs (Cannon et al. 2010). The current model is designed to estimate the probability of debris-flow likelihood as a response to a given peak 15-minute rainfall intensity. Two equations are used for debris flow prediction (Table 1). The x variable represents equation (1) and is used in the logistic regression equation (2) (Table 1). Equation (3) is used for volume predictions (Table 1).

Although debris flows may largely pose a safety concern, those that reach rivers may yield ecological benefits for certain salmonid species. In fact, debris flow sediment and gravel deposits may add spawning gravel to river beds. The deposits resulting from these natural flow processes are mimicked in gravel augmentation projects with the intended goal of supporting the spawning of salmonid species (Zeug et al. 2014; CalFed 2005). Salmonid species require various sizes of spawning gravel; our analysis of debris flow deposits will focus on gravel grain sizes that support the spawning of Steelhead trout (*O. mykiss*). The D_{50}, or the median diameter of particle size distribution, for Steelhead trout spawning gravel and redds has been reported to range from values as low as 10.4 mm to values as large as 46 mm (Kondolf and Wolman 1993).

Considering the relatively high variability in D_{50} values, studies have worked to model preferred spawning gravel size in relation to Salmonid species or fish length (Kondolf and Wolman 1993). In general, these studies aiming to relate spawning gravel size with fish size or species-specific attributes have found that salmonid fish species can utilize gravels that have a median diameter up to 10% of their body length (Kondolf and Wolman 1993). Studies monitoring the effects of gravel augmentation projects also describe relationships between fish size and spawning gravel. A study on the results of gravel augmentation suited for Steelhead trout found that individuals now require or prefer spawning gravel on the smaller side of their known spawning gravel ranges (Zeug et al. 2014).

Given gravel augmentation projects and debris flow deposits are not synonymous and the magnitude of similarity between the two varies based upon site-specific conditions, the effects of debris flows cannot be fully predicted by the results of gravel augmentation projects. However, if debris flow study sites are determined to replicate gravel augmentation, comparisons between the

two may be supported. Studies have been completed in which researchers identify the uncertainties related to gravel augmentation or manual sediment additions (CalFed 2005). One common issue faced after gravel augmentation is the mobilization of sediment additions downriver. Although dependent upon several factors including gravel characteristics, wave amplitude to flow depth ratio, and channel morphology, many studies analyzing the performance of gravel augmentation projects observe an expedited increase in bedload transport rates downstream of sediment wave crests (CalFed 2005). While sediment transport is inevitable, maximized temporal dispersion of gravel additions may be achieved with small and frequent spawning gravel deposits as opposed to large and infrequent additions that increase deposit spatial extent over time (CalFed 2005).

Debris flows resulting from wildfire events may contribute additions of spawning gravel similar to those from gravel augmentation deposits. Wildfires and their affiliated mass wasting events have occurred in many areas repeatedly. One such area is the Carmel River watershed located in Carmel, California. The Carmel River watershed has experienced multiple fires and mass wasting events. The Marble Cone Fire of August 1977 was an intense and extensive fire that burned a great section of the upper Carmel watershed (Hecht 1981). The fire was followed by heavy precipitation which induced post-fire runoff and a documented epicycle of filling and scouring (Hecht 1981). A fire of similar intensity, the Basin Complex Fire of 2008, also occurred in the upper Carmel watershed. Although the magnitude of the Basin Complex Fire resembled that of the Marble Cone Fire, a lack of heavy precipitation prevented the occurrence of post-fire debris flow events (Richmond 2009).

The Carmel River Watershed has experienced more recent wildfire events; the River Fire and the Carmel Fire both affected areas of the watershed, however the Carmel Fire was the influencing factor in our study site. The Carmel fire, burning from August 18, 2020 through September 4, 2020, burnt a total of 6,905 acres, including our study site, at moderate to low severity while causing significant property damage and destruction (WERT 2020). Our study site, located along the Carmel River just inland of the central California coast, begins 500 m downstream from the former San Clemente Dam and reservoir and ends 2000 m from the former dam (Figure 1).

Table 1. USGS predictive models and variable description (USGS 2021).

1) $x = -3.63 + (0.41 \times X1R) + (0.67 \times X2R) + (0.7 \times X3R)$ X1R is the proportion of upslope area classified as high or moderate soil burn severity and with gradients ≥ 23°, multiplied by the peak 15-minute rainfall accumulation of the design storm (in millimeters [mm]) X2R is the average differenced normalized burn ratio (dNBR) of the upslope area, multiplied by the peak 15-minute rainfall accumulation of the design storm (in millimeters [mm]) X3R is the soil KF-Factor (Schwartz and Alexander, 1995) of the upslope area, multiplied by the peak 15-minute rainfall accumulation of the design storm (in millimeters [mm]).
2) $P = e^x / (1 + e^x)$ P is the probability of debris-flow occurrence in fractional form, and e^x is the exponential function where e represents the mathematical constant 2.718.
3) $\ln(V) = 4.22 + (0.13 \times \sqrt{(ElevRange)}) + (0.36 \times \ln(HMkm)) + (0.39 \times \sqrt{(i15)})$ ElevRange is the range (maximum elevation–minimum elevation) of elevation values within the upstream watershed (in meters) HMkm is the area upstream of the calculation point that was burned at high or moderate severity (in km2) i15 is the spatially-averaged peak 15-min rainfall intensity for the design storm in the upstream watershed (in mm/h)

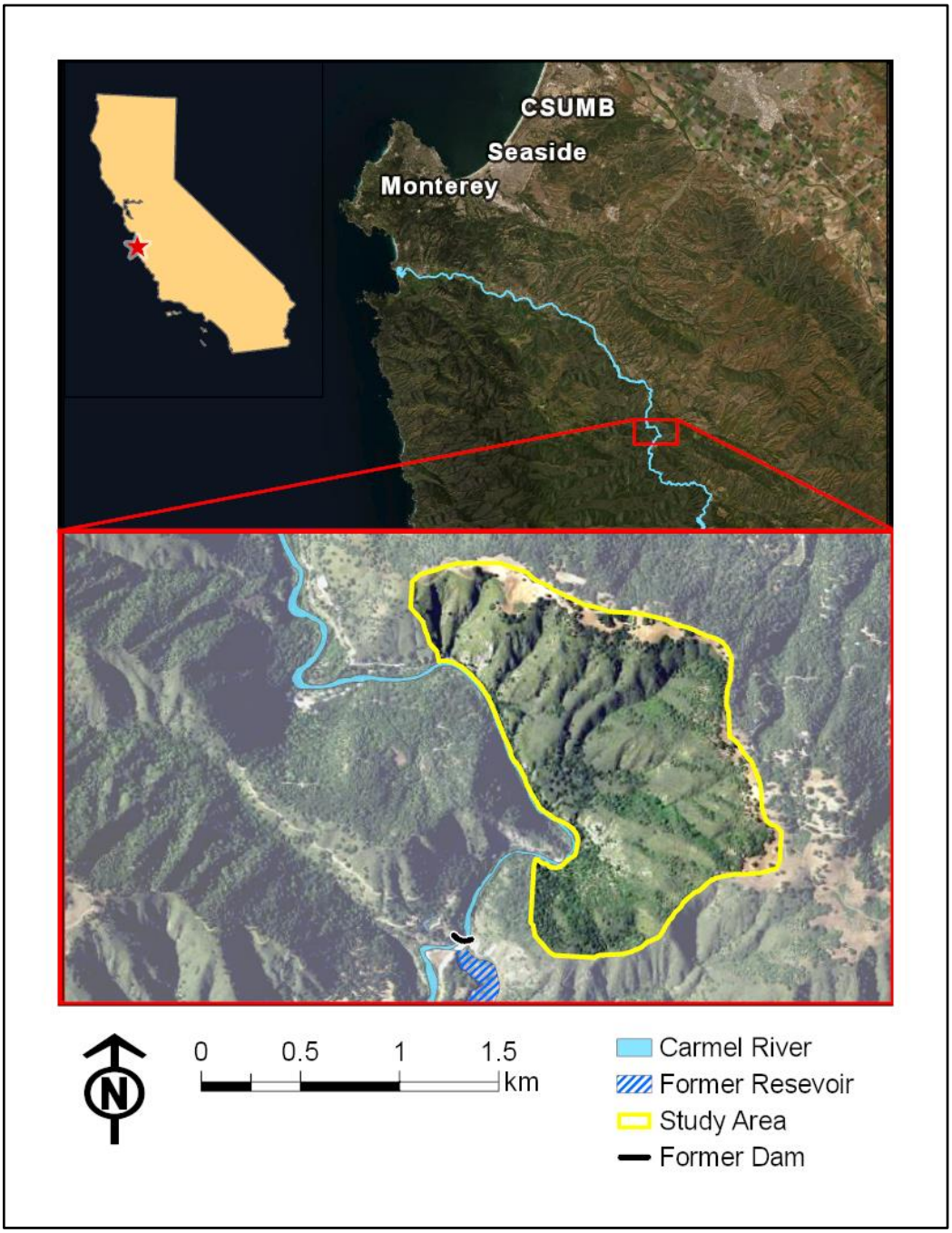

Figure 1. Location of the study site along the Carmel River south of Monterey, CA.

Historically, wildfires and natural mass wasting events like debris flows have not been the sole factors influencing spawning gravel availability at our study site. The removal of the San Clemente Dam, the largest dam removal project in California, had a profound effect on spawning gravel abundance. Studies evaluating the effects of the dam removal on spawning gravel have determined that spawning gravel amounts in the Carmel River have significantly decreased since dam deconstruction in 2015 (Figure 2; Harrison et al. 2018, Chow et al. 2016, TetraTech 2016). This severe decrease in spawning gravel abundance may be attributed to the river reconstruction process, which roughly consisted of a river reroute, sediment trapping and reservoir isolation, weir and riffle pool construction, and plunge pool construction (TetraTech 2016; Smith et al. 2020).

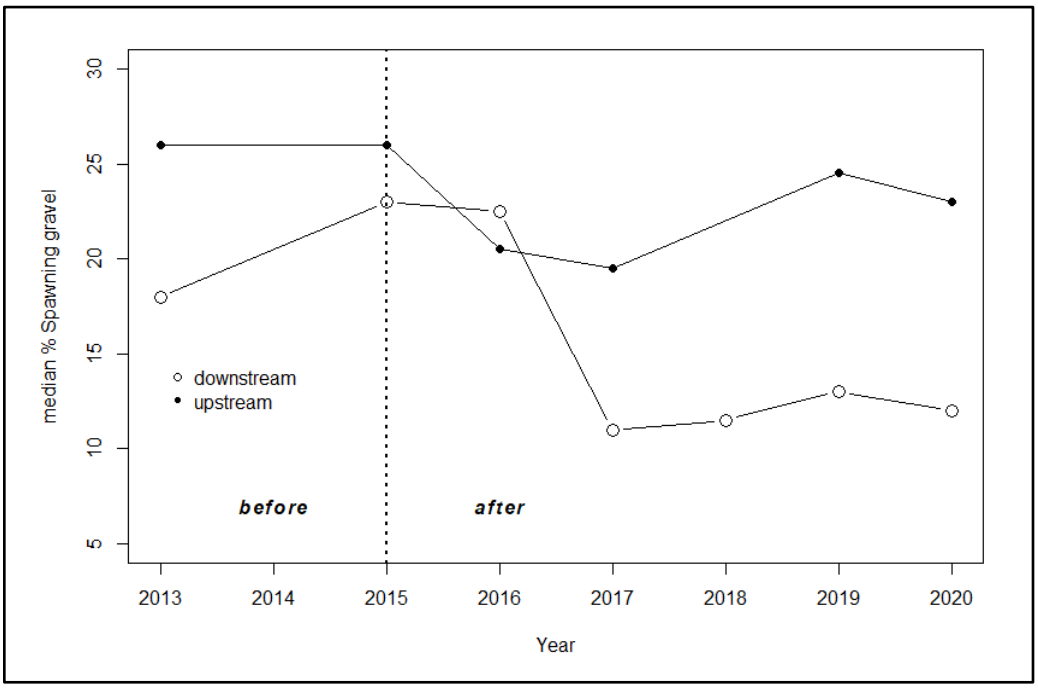

Figure 2: Changes in percent spawning gravel upstream and downstream of the San Clemente Dam before and after its removal in 2015. The upstream data may be interpreted as the "control" in a Before-After-Control-Impact analysis

One objective of our study is to evaluate the USGS predictive model for debris flow triggering rainfall intensity, debris flow probabilities and debris flow volumes. The second objective is to determine if post-wildfire debris flows triggered by the rainfall event of January 2021 had any contribution to percent salmonid spawning gravel in the Carmel riverbed. The 2020

Carmel Wildfire provided a unique opportunity to study post-wildfire debris flow events in combination with the recent San Clemente Dam removal. With post-wildfire conditions in mind, we were able to capture images of our study site before and after debris flow events, as well as post-wildfire debris flow measurements. This approach enabled a per basin evaluation of established USGS predictive modeling for material discharge in our study site. We also assessed riverbed spawning gravel before and after the debris flow events to evaluate their contribution of spawning gravel to the Carmel River.

2 Methods

Game Cameras and Rain Gauges

Game cameras (Figure 3) were secured to trees at the mouths of basins HI and JK (Figure 4), and a 0.2 mm event-based tipping rain gage was installed prior to a forecasted January 27th, 2021 high intensity rain event. The game cameras were set to take photos in 15-minute intervals. Following the storm, time-stamped images were recovered from the game cameras, and precipitation data were retrieved from the Onset RG3-M rain gage. The rain gauge was located 732 m and 886 m, respectively from the two game cameras. Time stamps from game camera photos were cross-referenced with precipitation data to determine precipitation intensity at the time of the debris flows. Continuous 15-minute precipitation intensities were calculated from the rain gage record to determine the intensity required to trigger debris flows from the study site slopes.

Figure 3. Game camera set up to face basin mouth.

Data Visualization: ArcGIS and Mapping

To depict the susceptibility certain areas had for mass wasting events, data describing landslide potential, soil type, burn severity, erosion, and geology of our study site were imported and analyzed in ArcGIS Pro. Layers and shapefiles pertaining to landslide potential, soil type, geology and erosion were clipped to the study site boundary and additionally processed or emphasized using common ArcGIS Pro functions such as feature class creations or rasters if required. Maps were generated after processing and formatting to depict the study site basins according to each of these analysis factors.

The extents of the debris flow deposits were mapped in ArcGIS Pro using techniques and tools, including inverse distance weighted (IDW) interpolation, raster calculations, and clipped polygons. Post-wildfire debris flow deposits at the mouths of basins A-L (Figure 4) were surveyed using a total station (Figure 5) to create a non-georeferenced continuous surface digital elevation model (DEM). Data collected during these total station field surveys served as the basis for our generated maps. Using the survey data and relevant ArcGIS Pro tools, we defined the extent of each basin's debris flow relative to the Carmel River and used a bathymetric color scale to categorize the elevation of each flow deposit. The thickness of each debris flow was determined as the difference between the pre-debris flow (2018) LiDAR DEM and debris flow surface DEM. Debris flow deposit volume was found by multiplying the average thickness with the surveyed deposit area. Debris flow mapping following this process was completed for basins A-K. Deposit extent maps were not generated for basins L and M. The debris flow deposit related to basin L was of negligible size while basin M did not produce a debris flow deposit.

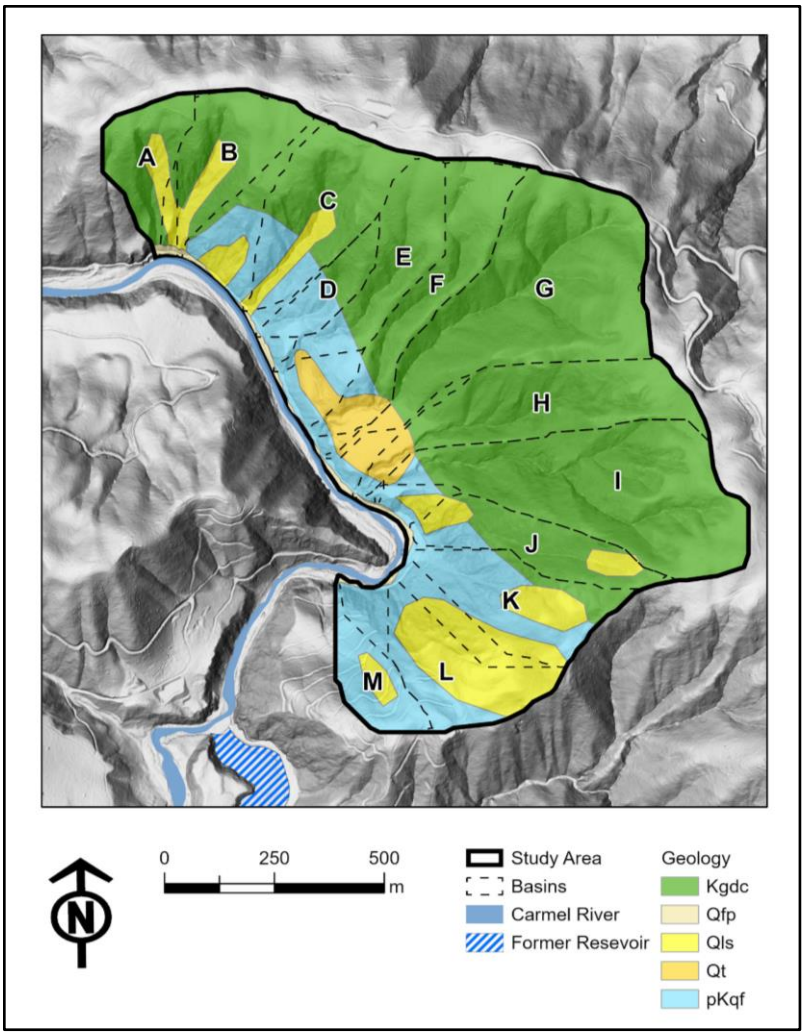

Figure 4. Map of study basins and geologic rock units. Letters are small watersheds (basins) described in the text. Basins F and G formed a single combined deposit, as did basins H and I. Kgdc: Cretaceous Granodiorite; pKqf: preCretaceous metamorphic rocks; Qfp: Quaternary floodplain deposits; Qls: Quaternary landslides; Qt: Quaternary terraces. Geologic data from Rosenberg (2001)

Figure 5. Total station surveys of the basin deposits. Deposit shown are at the mouth of basin K.

Spawning Gravel Fieldwork

To determine the effects of debris flows on spawning gravel availability in the Carmel River, gravel grain size measurements were collected for statistical analysis from each debris flow deposit terminous (snout) where it was adjacent to the Carmel River. The process of collecting the grain size data started with height and width measurements at each individual debris flow snout. These measurements were used to calculate the snout area and the width along which to conduct grain size sampling. The total width of the debris flow snout was divided by five to determine the location along the transect at which each quadrat would be placed for collection. A 'W' pattern was chosen for sampling along each transect using a square meter sized quadrat to ensure that the full stratification of gravel within the debris flow deposits was encompassed by our samples. The gravel grain size was measured by a standard gravelometer with measurement categories including less than: 2mm, 2.8mm, 5.6mm, 8mm, 11mm, 16mm, 22.6mm, 32mm, 45mm, 64mm, 90mm, 128mm, 180mm, 256mm and 300mm. Each transect, with the exception of Basin D, resulted in 120 gravel grain size counts. Basin D had a significantly smaller snout area compared to the rest

of the basins; only three quadrat measurements could be taken, which produced a total of 60 grains sampled in the transect.

Spawning Gravel Analysis

Grain size counts from all of the debris flow snouts were compiled into a spreadsheet to calculate the D50, snout area (m2), graphical mean, and percent spawning gravel for each basin. Grain size percentiles were determined by plotting grain size counts against cumulative percent of the sample on log transformed axes. These plots were used to find the sixteenth, fiftieth, and eight-fourth percentiles (D16, D50 and D84) of each basin's associated deposit. Those values were converted into the standard units of the Krumbein phi scale to calculate the graphical mean. Percent spawning gravel was also calculated for each basin by dividing the total gravel counts that fell within the spawning gravel range for Steelhead trout (32 to 90 mm) by the total number of gravel counts conducted at each transect. These calculations were completed for each basin and averaged together to represent the entire study area.

3 Results

Geology

Analysis of the underlying basin geology showed that the majority of the upper areas of basins A-J consisted of Cretaceous granodiorite *(*Figure 4). The lower areas of basin C-J consisted of gneiss. Basins K-M were almost entirely composed of gneiss. Quaternary landslide deposits were seen in basins A, B, C, J, K, L, and M. These landslide deposits consisted of debris from previous hillslope failures during the Holocene. Quaternary terrace deposits were seen in basins E-I, which were older fluvial terrace deposits from the Pleistocene. Quaternary floodplain deposits were seen along the road by the basin mouths and the current Carmel River floodplain.

Soil Types

Basins A - K are primarily composed of gravelly sandy loam (Figure 6). As shown by the soil ternary diagram (Figure 7), sandy loam consists of 0% to 50% silt, 50% to 70% sand, and 15% to 20% clay. Most basins in our study site contain approximately 17% clay. Basin M and half of basin L contain 32% percent clay, and the upper portions of basins B- J contain 24% to 28% clay

(Figure 8). This allows these sections to be categorized in the sandy clay loam category rather than the sandy loam category. Our study site contains three different drainage classifications: drainage type A has a low runoff potential when wet, drainage type B has a moderately low runoff potential when wet, drainage type C has a moderately high runoff potential when wet (Figure 9) (USDA 2007).

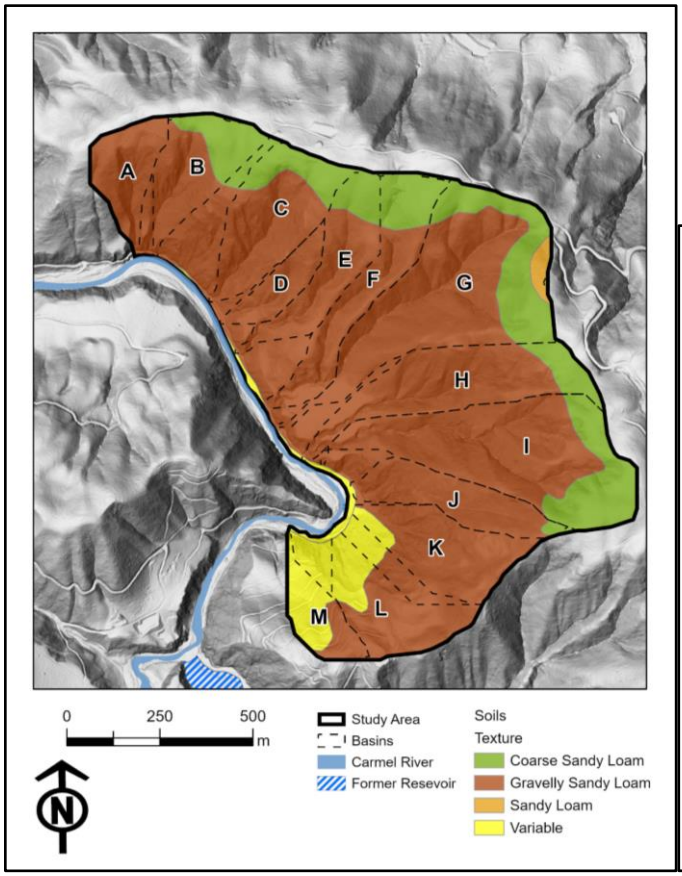

Figure 6. Map of the soil textures present within our study area. Geologic data from Rosenberg (2001)

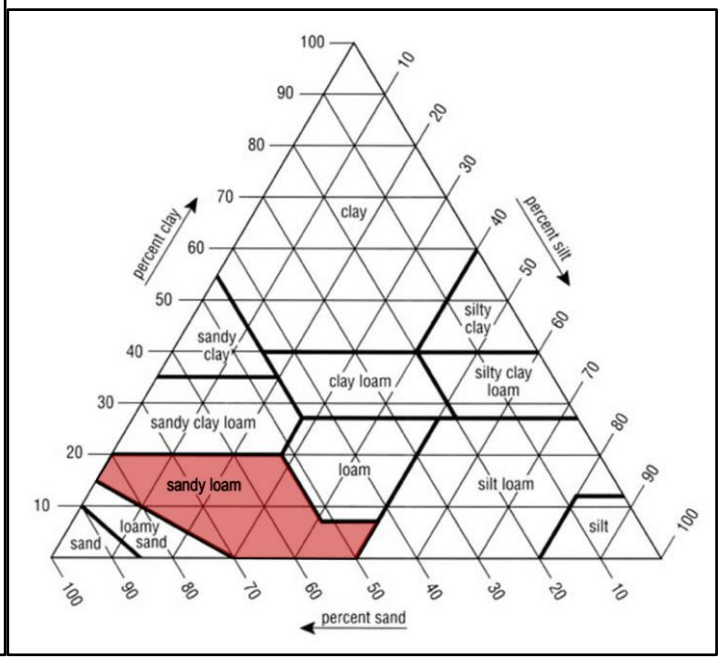

Figure 7. Soil ternary diagram with our study area's soil type in red.

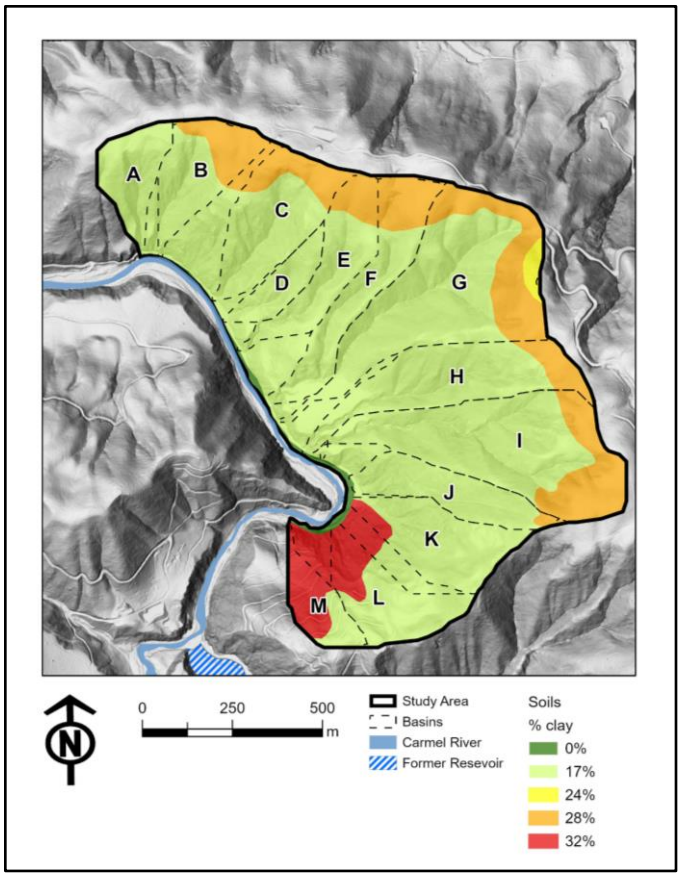

Figure 8. Clay content of soils within our study area. Geologic data from Rosenberg (2001).

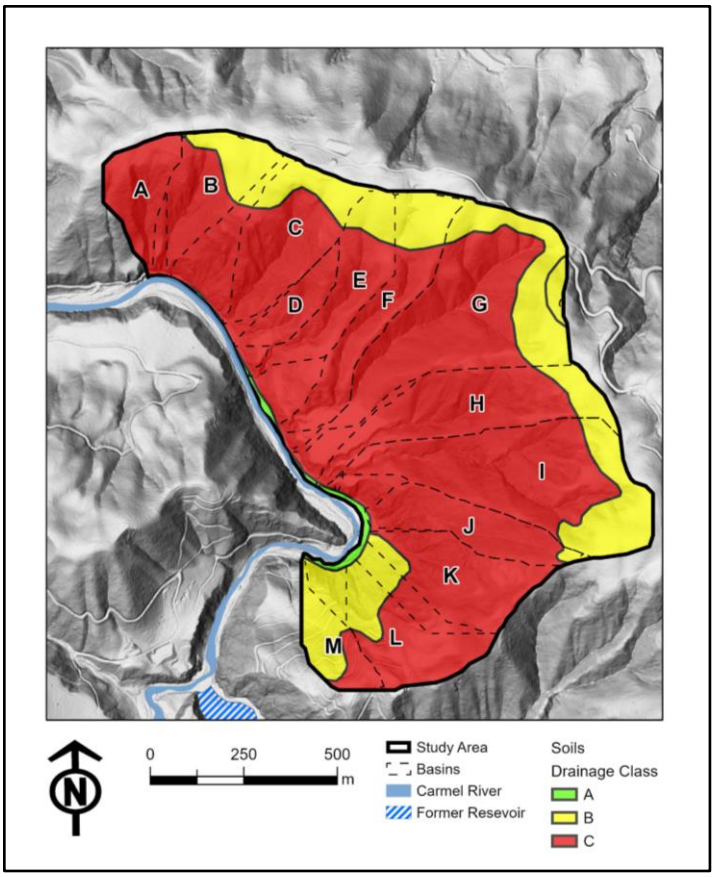

Figure 9. Soil drainage classes within our study area. Geologic data from Rosenberg (2001).

Hazard Risks

All of the basins were found to have high erosion potential (Figure 10). Our study site was determined to have high, moderate, and low landslide susceptibility potentials (Figure 11). The risk for landslides is particularly high in basins K, L, and M and in the lower parts of basins A, B, HI, and J. However, there is a low risk for landslides in basins C, D, E and majority of basins, A, B, FG, HI, and J. This could be due to the soil composition in those basins. Our study site did not contain any severely burned areas; most areas were classified as having moderate burn severity (Figure 12).

Debris Flow Deposit Extents

A strong precipitation event peaking early on January 27, 2021 produced a total of 17 slope failure events (Figure 13). Seven of the events were not predicted by the USGS model. The unpredicted events were 5 rockfalls (Figure 14) and 2 debris flows (Figure 15). The debris flows from all basins and the unpredicted flows and rockfalls produced a total of 2542 cubic meters of gravelly deposits (Table 2). Basins HI produced the largest deposit volumes at 990 cubic meters (Figure 16). Basin K produced the second largest deposit of 721 cubic meters (Figure 17). Basins FG only produced a deposit of 11 cubic meters, the smallest deposit of all the basins studied (Table 2). The remaining deposit extent maps can be found in the appendix.

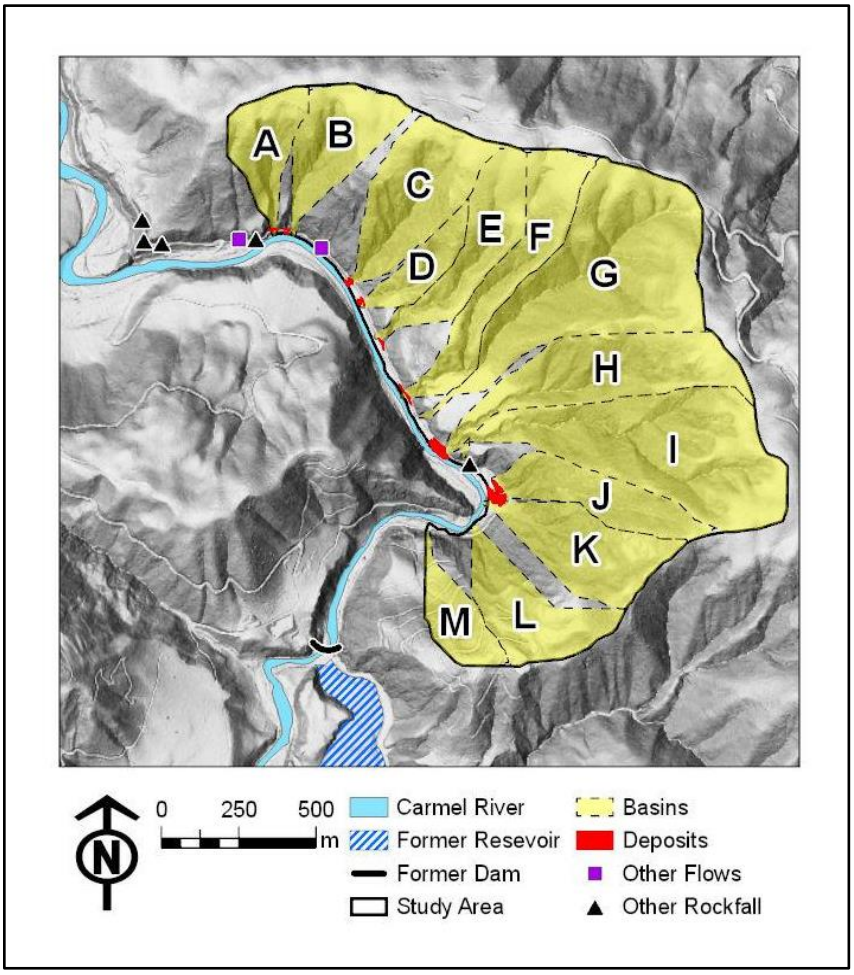

Figure 13. Location of deposits within our study area. Locations of "other" flows and rockfalls, not predicted by the USGS models are also shown.

Figure 14. Rockfall 5 located between basins HI and J

Figure 15. Unpredicted flow 2 located between basins B and C. Dry ravel was present before and after the rain event

Table 2. Inventory table containing attributes of each flow or rockfall.

Post-Fire Rock Fall and Debris Flow Events
Carmel Fire
Sleepy Hollow

Debris flow (DF)
Landslide (LS)
Rock Fall (RF)

									USGS predictions				
Event no.	Basin	UTM_easting (m)	UTM_northing (m)	runout_distance (m)	feature type	deposit_area (m^2)	deposit_vol (m^3)	Dist to gage (m)	Shape Area	PCI Legend	Volume	VolMin	VolMax
1	A	615598	4034148	15	DF	105	24	278	39200	20-40%	372	46	2978
2	B	615634	4034149	14	DF	108	61	314	57300	20-40%	633	79	5066
3	C	615808	4034021	14	DF	255	171	488	80700	40-60%	1031	129	8256
4	D	615836	4033969	23	DF	197	35	515	24700	60-80%	653	82	5224
5	E	615891	4033862	14	DF	144	38	571	59600	40-60%	822	103	6583
6	FG	615961	4033721	9	DF	194	11	641	253900	40-60%	3105	194	12425
7	HI	616053	4033597	26	DF	1176	990	732	269100	60-80%	4772	298	19097
8	J	616206	4033486	44	DF	486	182	886	50900	60-80%	1259	157	10079
8	K	616212	4033463	51	DF	1400	721	892	69900	60-80%	1497	187	11986
9	L	616137	4033380	49	DF	172	30	817	59200	20-40%	831	104	6650
10	M	615981	4033390	0	NA	NA	NA	1010	31000	20-40%	506	63	4053
11	Rockfall1	615258	4034166	4	RF	85	3	63					
12	Rockfall2	615260	4034119	3.5	RF	20	5	60					
13	Rockfall3	615311	4034108	3	RF	15	5	11					
14	Rockfall4	615553	4034120	4	RF	30	6	233					
15	Rockfall5	616118	4033554	5	RF	40	30	798					
17	Flow1	615509	4034119	40	DF	180	80	189					
18	Flow2	615725	4034100	15	DF	116	150	405					
						sum of vol=	2542						

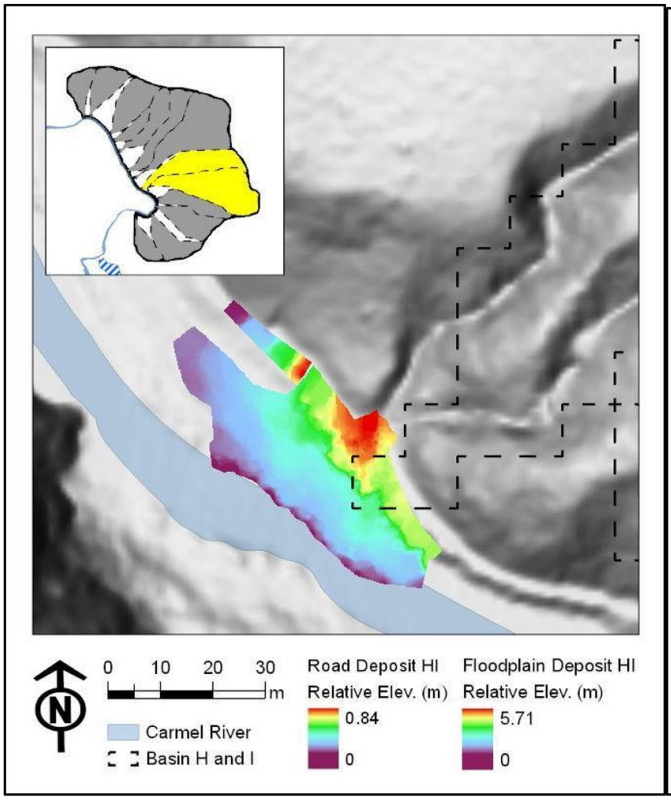

Figure 16. Map view of the deposit extent produced by basin H and I.

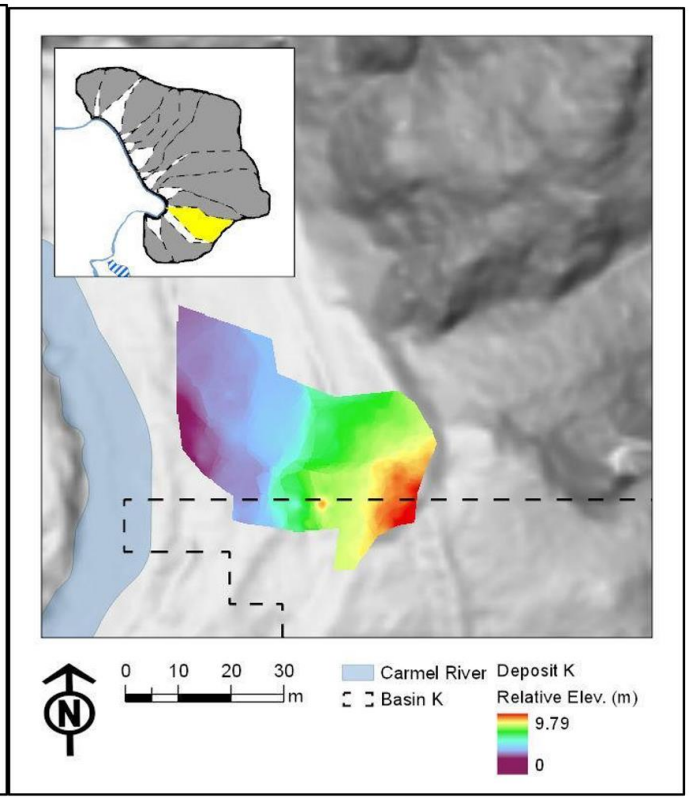

Figure 17. Map view of the deposit extent produced by basin K.

Precipitation Intensity

The timing of the rainfall intensity triggering the slope failures was constrained to have occurred between 0315 hr and 0330 hr on January 27 as observed using two game cameras that recorded the debris flow events simultaneously. During the 15-minute interval within which debris flows occurred, 15 minute duration rain intensities exceeding 24 mm/hr were observed, with a maximum 15 minute intensity of approximately 34 mm/hr (Figure 18).

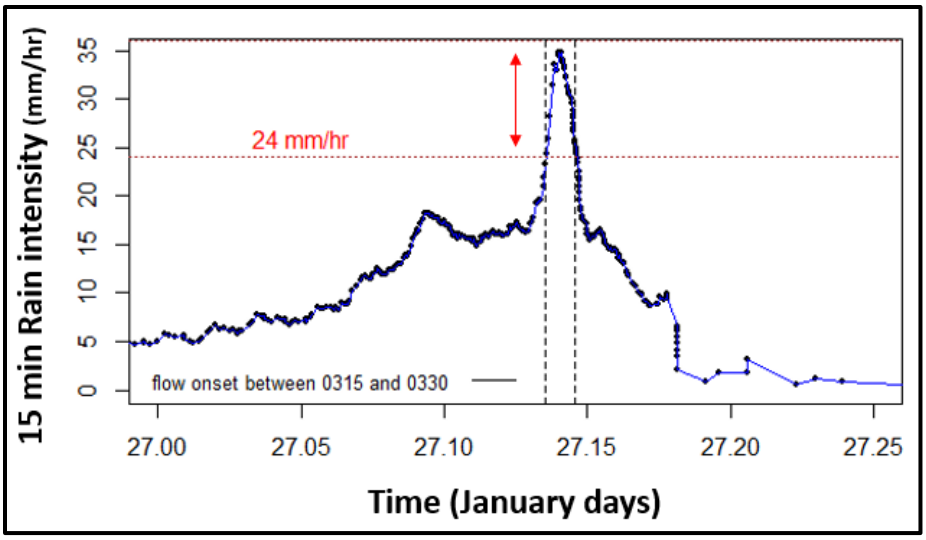

Figure 18. 15-min rainfall intensity during the debris flow triggering rain event (vertical dashed lines).

Spawning Gravel

Each debris flow deposit, with the exception of the basin D debris flow deposit, had a D_{50} within the spawning gravel range for Steelhead trout (32-90 mm) (Table 3). Each basin's debris flow deposit contained at least 36% spawning gravel. The debris flow deposit associated with basin A contained the highest concentration of potential spawning gravel, at 64% (Table 3). Differences in debris flow deposit snout characteristics such as area could account for the variability in percent spawning gravel between sites. Cumulatively, all debris flow deposits had a D_{50} of 50 mm, a graphical mean of 48.5 mm, an average percent spawning gravel of 45.8%, and a total snout area of 240.9 m^2.

The median grain size of all deposits combined was approximately 53% (left box in Figure 19). Although many of the debris flows contributed spawning-sized gravel to the Carmel River, visual inspection of the river bed at each debris flow site showed that virtually no new spawning gravel was present. The condition of the river bed is represented by grain size counts taken 400 m upstream of the debris flow locations (right box in Figure 19). When comparing grain sizes in undisturbed channel sites to those in the debris flows, there is a statistically significant difference in percent spawning gravel. A Welch's t-test was used to compare the spawning gravel abundance in the undisturbed channel sites and the spawning gravel abundance in the sites that experienced debris flows, resulting in a p-value of 0.006. This comparison underscores the result that the

existing Carmel River channel is very low in spawning gravel abundance, whereas the debris flows are enriched in spawning-size gravel.

Table 3. Spawning gravel measurements.

Deposit	D_{50}	Graphical Mean (phi)	% Spawning Gravel	Snout Area (m^2)
A	46	48.4	64.2	25.6
B	60	67.8	36.7	20.8
C	50	53.6	38	40
D	28	34.6	46.7	6
FG	55	68.6	44	148.5
Total	50	48.5	45.8	240.9

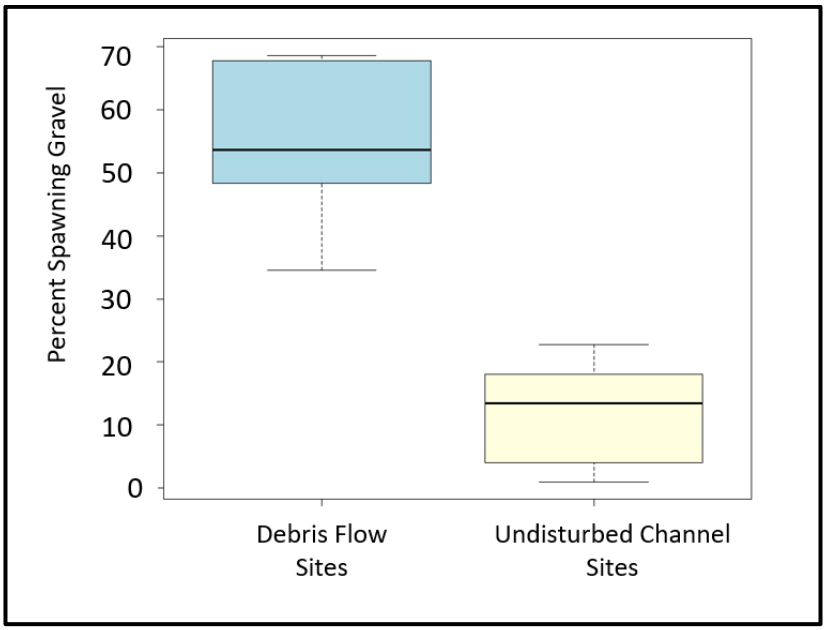

Figure 19. Percent spawning gravel in debris flows compared to undisturbed Carmel channel sites.

4 Discussion

Precipitation Intensity

Debris flow activity commenced once the 15-minute duration rainfall intensity exceeded 24 mm/hr (Figure 18). This value is precisely predicted by the USGS model. The exact triggering rainfall threshold could not be determined as the game cameras recorded photos only every 15 minutes. During the 15-minute interval that debris flows occurred, rain intensities exceeding 24 mm/hr were observed with a maximum intensity of approximately 34 mm/hr (Figure 18).

USGS Debris Flow Predictions

The January 27th 2021 storm incident produced a total of 17 slope failure events, ten of which were projected by the USGS model. Of the 7 unpredicted events, 5 were rockfalls (rather than debris flows) and 2 were debris flows. Debris flows were observed from all but one of the basins predicted to experience debris flows by the USGS model. Four out of ten of the studied debris flow deposit volumes were captured by the USGS confidence intervals.

The USGS model correctly predicted debris flow events for all basins but one (basin M; Figure 20). Basins A-L all experienced debris flow events as predicted by the model. Rock falls were observed from basins with areas that were smaller than the 0.2 km^2 minimum threshold used in the USGS predictive model. Due to the USGS model's minimum basin size requirement, the model did not account for a total of five rockfalls and two debris flows in the study site.

Upon analyzing the USGS predictions and the field measured volume deposits, we found the deposits to be less than what was projected by the USGS (Figure 20). This may be partially explained by sediment transport during high river flows that followed the precipitation event. Of the ten debris flows predicted by the USGS model, eight of them (A-K) terminated in the Carmel river while one (basin L) terminated on the road adjacent to the river. Steep angular facets were observed at debris flow snouts that reached the river. This indicated that a portion of the debris flow materials had been eroded during the high flow events in the Carmel River. This partial debris flow erosion may account for the differences between USGS model predictions and the observed basin volumes.

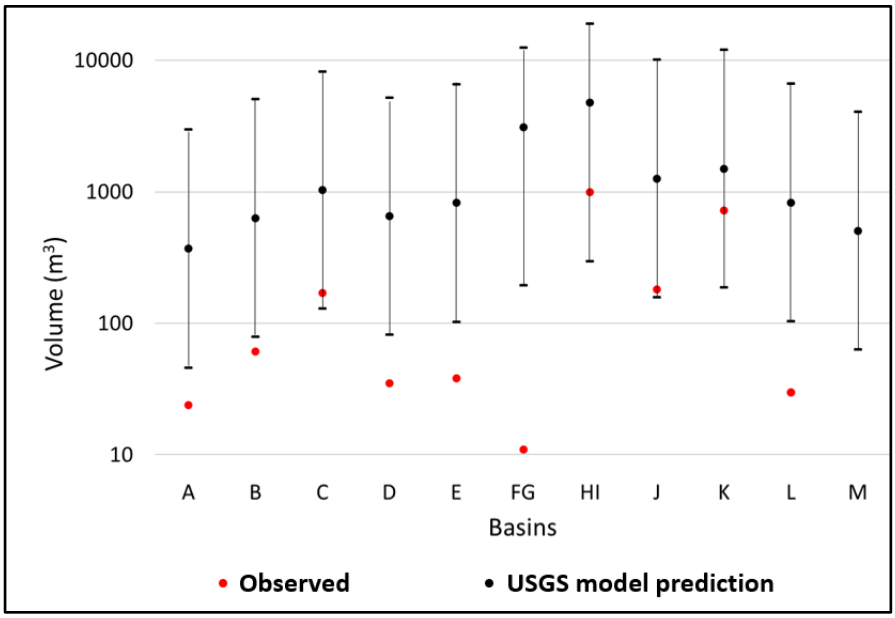

Figure 20. Chart comparing observed debris flows and volumes in basins with USGS predicted events. The black dots and whiskers indicate the averages and the 95% confidence intervals for the USGS model volume predictions. The red dots indicate observed volumes. Basin M produced no debris flows.

To measure the correlation between the field data and the USGS projections, a regression analysis was conducted between the estimated volume recorded from our field survey and the projected average of each basin. Based on the resulting P-value of 0.02 and an R-squared value of 0.51, a moderate correlation was found between the average volume projections and the average volume measurements from the field survey. This indicates that although estimated volumes, on average, were less than the volumes predicted by the USGS model, debris flow volumes accurately followed the overall trend that was predicted.

Spawning Gravel

The post-fire debris flows observed at our study site were evaluated in order to determine if they delivered spawning gravel consistent with sizes required by Steelhead trout. Gravel counts conducted on the debris flow deposits and statistical analysis of this field survey data support the conclusion that the studied flows contained moderate to high concentrations of potential spawning gravel (Figure 19). The cumulative D50, 50 mm, falls within the general range of spawning gravel

values known for Steelhead trout and the specific size range used by Steelhead in the Carmel River, which is 10-80 mm (Kondolf and Wolman 1993).

Although statistical analysis suggested a uniformly robust distribution of potential spawning gravel into the river during the debris flow events, qualitative evaluation indicated that no significant amount of spawning sized gravel was deposited into the river and available for Steelhead use. The discrepancy between observations and analytical results related to spawning gravel abundance in our study site may be accounted for by the redistribution of spawning gravel deposits by peak runoff that arrived at the site after the debris flows were triggered. Debris flows from basins A, B, D, and JK did not reach the river banks. This study determined that although the post-fire debris flows contained a significant amount of suitably sized gravel for Steelhead trout spawning, the lack of gravel abundance and sediment bar formation observed during site visits suggests that the introduced gravel did not improve conditions for steelhead spawning.

Aside from debris flows, increased fluvial discharge rates have the ability to deliver significant volumes of spawning gravel. Past findings describe high flow events dispersing river bank gravel deposits as a source of suitable spawning gravel (Harrison et al. 2018).

Debris Flow Processes

Prior to the rain event, the basin channels were full of colluvium (Right box of Figure 21). After the high-intensity rain event, many channels had eroded to the granodiorite bedrock (Left box of Figure 21).

Figure 21. Red arrow indicates a portion of the bassin H channel. Blue arrow indicates a portion of the bassin I channel. Before (left) shows the pre-debris flow channels full of colluvium. Post-debris flow after channels eroded to bedrock (right).

Rilling and gullying were observed over the majority of the study area (Figures 22 and 23). This process is consistent with runoff-dominated sediment erosion rather than soil-slip slope failure. This type of erosion is known to originate from a lack of soil infiltration due to intense burns (Cannon et al. 2000). No scarring was observed that would indicate infiltrated soil-slip type debris flows.

Figure 22. Rilling and Gullying was observed in the majority of basins.

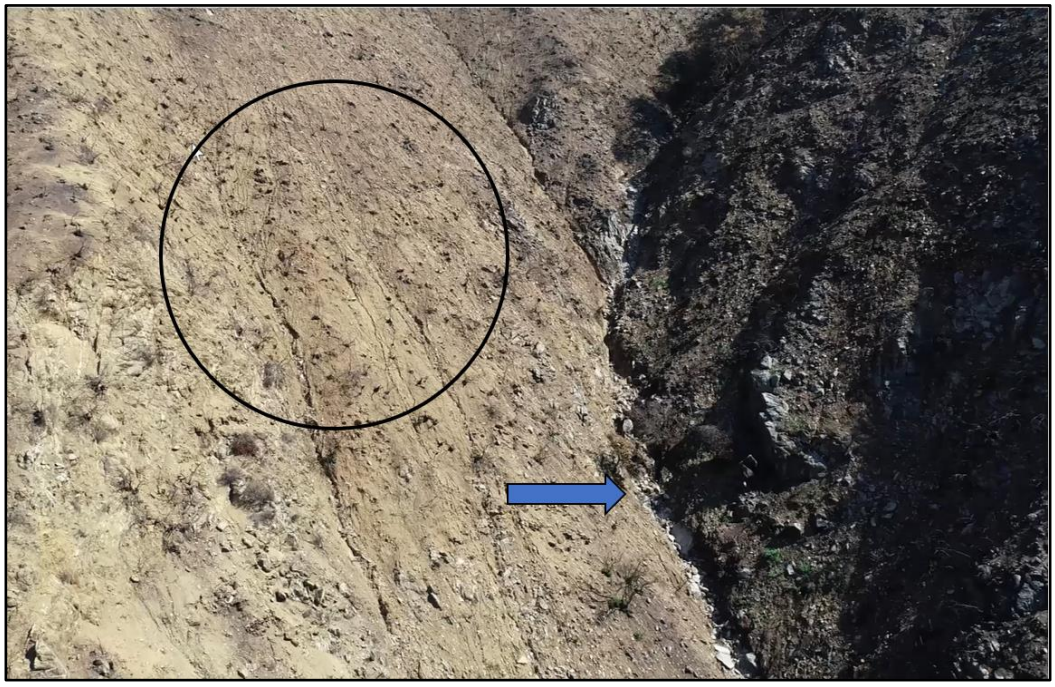

Figure 23. Circle indicates Rilling and Gullying. The arrow shows a channel from basin I eroded to bedrock.

5 References

1. Calfed. 2005. Key Uncertainties in Gravel Augmentation: Geomorphological And Biological Research Needs For Effective River Restoration. 1-91.

2. Cannon SH, Gartner JE, Rupert MG, Michael JA, Rea AH, Parrett C. 2010. Predicting the probability and volume of post-wildfire debris flows in the intermountain western United States. Bulletin of the Geological Society of America.

3. Cannon SH, Kirkham RM, Parise M. 2000. Wildfire-related debris-flow initiation processes, Storm King Mountain, Colorado. Amsterdam (NL): Geomorphology. 39(3–4):171–188

4. Costa JE. 1984. Developments and Applications of Geomorphology in Denver, Co. Berlin (DE): Springer.

5. Chow K, Fields J, Flores S, Hart K, Kleven A, Luna L, MacCarter L, and Smith D. 2016. San Clemente Dam Removal Sediment Impacts: Year One Report. Monterey (CA): Watershed Institute, California State University Monterey Bay. 1-38.

6. Harrison LR, East AE, Smith DP, Logan JB, Bond RM, Nicol CL, Williams TH, Boughton DA, Chow K, Luna L. 2018. River response to large-dam removal in a Mediterranean hydroclimatic setting: Carmel River, California, USA: River response to large-dam removal. Earth surface processes and landforms. 43(15):3009–3021.

7. Hecht B. 1984. Sequential changes in bed habitat conditions in the upper Carmel river following the marble-cone fire of august, 1977. In: California Riparian Systems. Oakland (CA): University of California Press. 42–49.

8. Kondolf GM, Wolman MG. 1993. The Sizes of Salmonid Spawning Gravels. Water Resources Research. 29(7):2275–2285.

9. Richmond S. 2009. Post-fire channel response: A comparison between the 1977 Marble Cone Fire and 2008 Basin Complex Fire on the upper Carmel River.

10. Rosenberg, L. 2001. Geologic resources and constraints Monterey county California. County of Monterey Environmental Resource Policy Department.

11. Schwartz GE, Alexander RB. 1995. Soils data for the conterminous United States derived from the NRCS State Soil Geographic (STATSGO) Database: U.S. Geological Survey Open-File Report. 95–449.

12. Scientific Background. Usgs.gov. https://www.usgs.gov/natural-hazards/landslide-hazards/science/scientific-background?qt-science_center_objects=0.

13. Smith, D. P., Kortman, S. R., Caudillo, A. M., Kwan-Davis, R. L., Wandke, J. J., Klein, J. W., Gennaro, M. C. S., Bogdan, M. A., and Vannerus, P. A. (2020) Controls on large boulder mobility in an “auto-naturalized” constructed step-pool river: San Clemente Dam removal and reroute project, Carmel River, California, USA. Earth Surf. Process. Landforms, https://doi.org/10.1002/esp.4860.

14. Staley DM, Negri JA, Kean JW, Laber JM, Tillery AC, Youberg AM. 2016. Updated logistic regression equations for the calculation of post-fire debris-flow likelihood in the western United States: U.S. Geological Survey Open-File Report 2016–1106: 1-13.

15. USDA 2007.Usda.gov. https://directives.sc.egov.usda.gov/OpenNonWebContent.aspx?content=17757.wba#:~:text=Group%20D%E2%80%94Soils%20in%20this,have%20high%20shrink%2Dswell%20potential.

16. Usgs.gov. https://pubs.usgs.gov/of/1998/0579/pdf/fskn_dmu.pdf.

17. Watershed Evaluation Response Team (WERT). CEU-BEU_004024 and CA-BEU-004081. 2020.

18. Westerling AL, Hidalgo HG, Cayan DR, Swetnam TW. 2006. Warming and earlier spring increase in western U.S. forest wildfire activity: Science 313: 940–943. doi: 10.1126/science.1128834.

19. Zeug SC, Sellheim K, Watry C, Rook B, Hannon J, Zimmerman J, Cox D, Merz J. 2014. Gravel augmentation increases spawning utilization by anadromous salmonids: A case study from California, USA: Gravel augmentation and Salmonid spawning. River research and applications. 30(6):707–718

6 Appendix: Debris Flow Deposit Maps

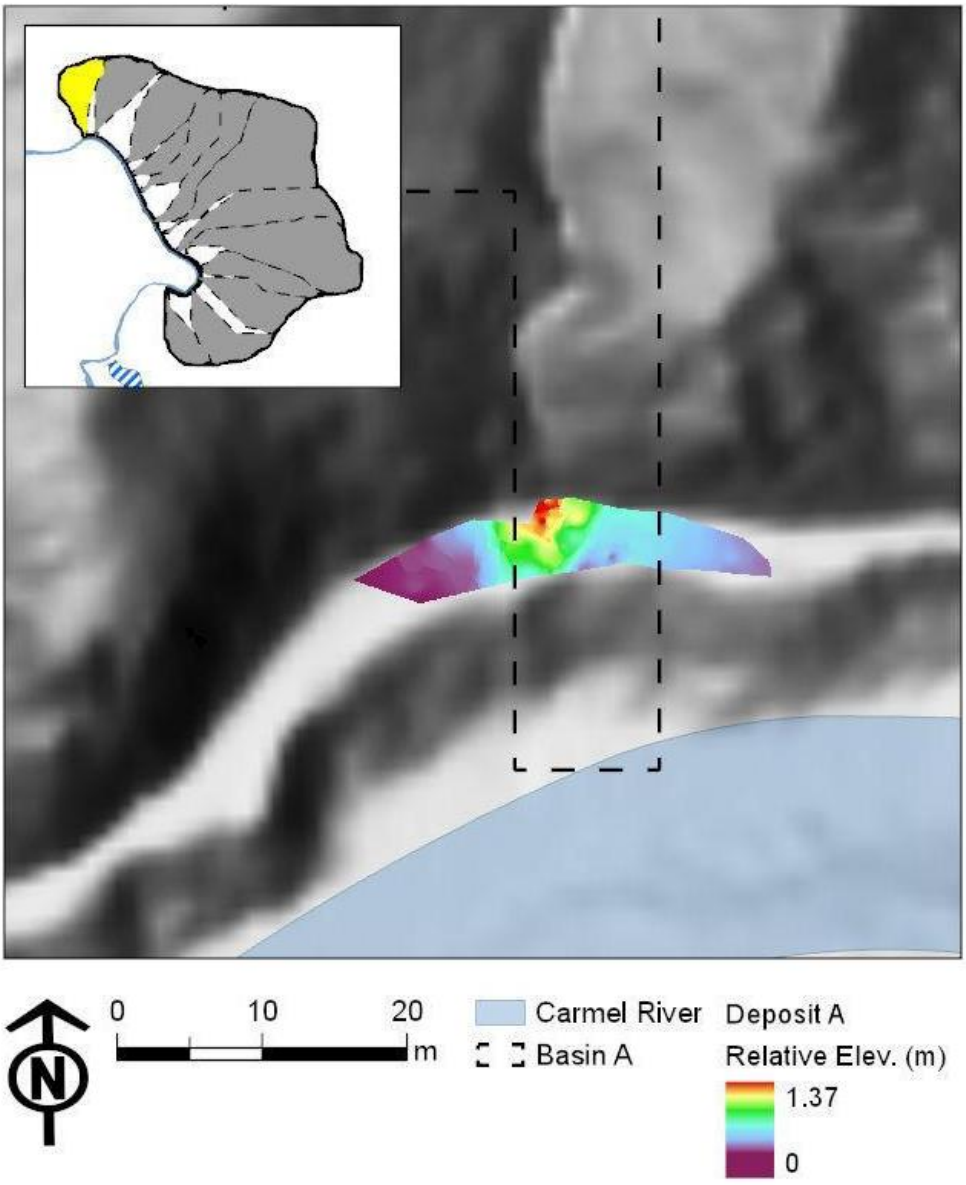

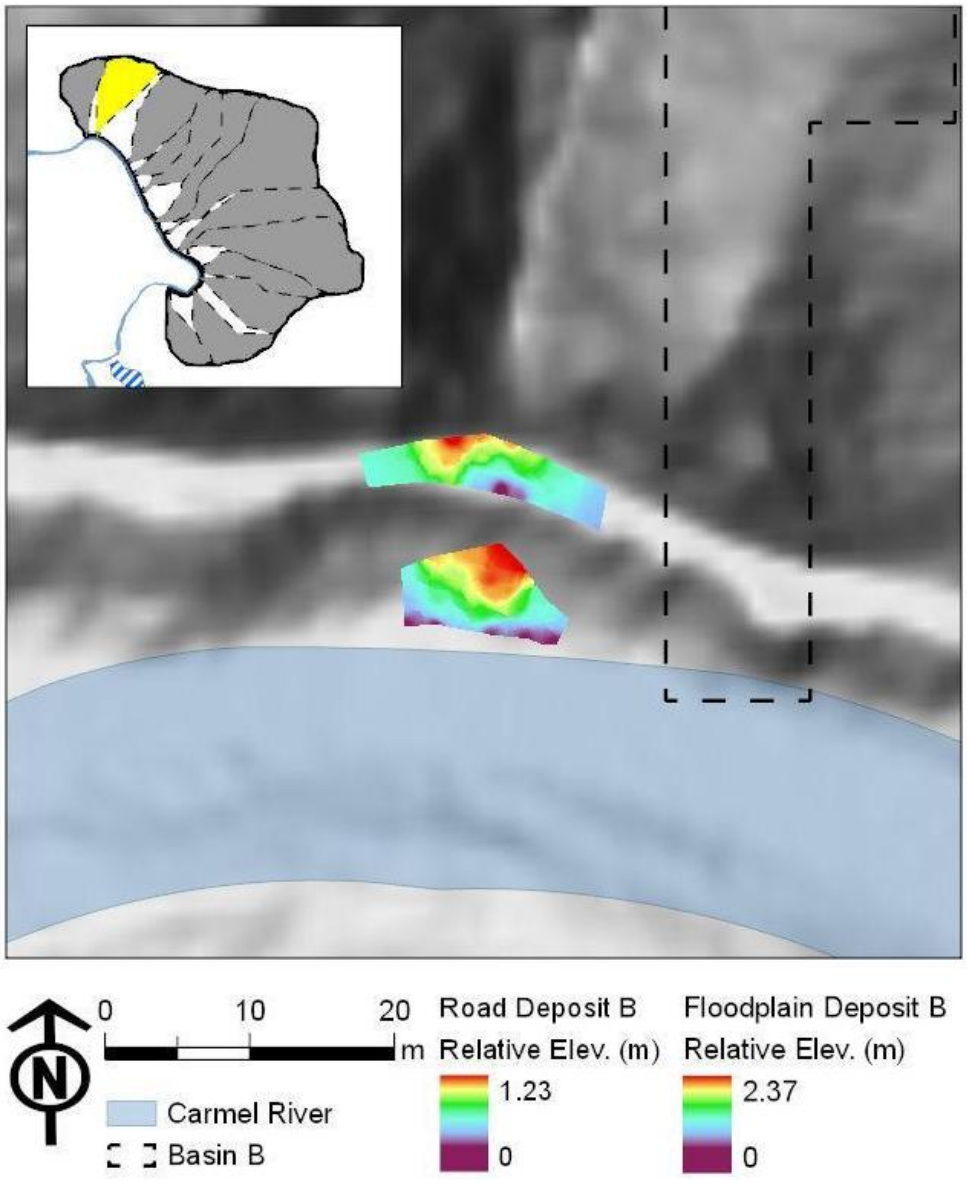
0
10
20
m
N
Carmel River
Basin B
Road Deposit B
Relative Elev. (m)
1.23
0
Floodplain Deposit B
Relative Elev. (m)
2.37
0

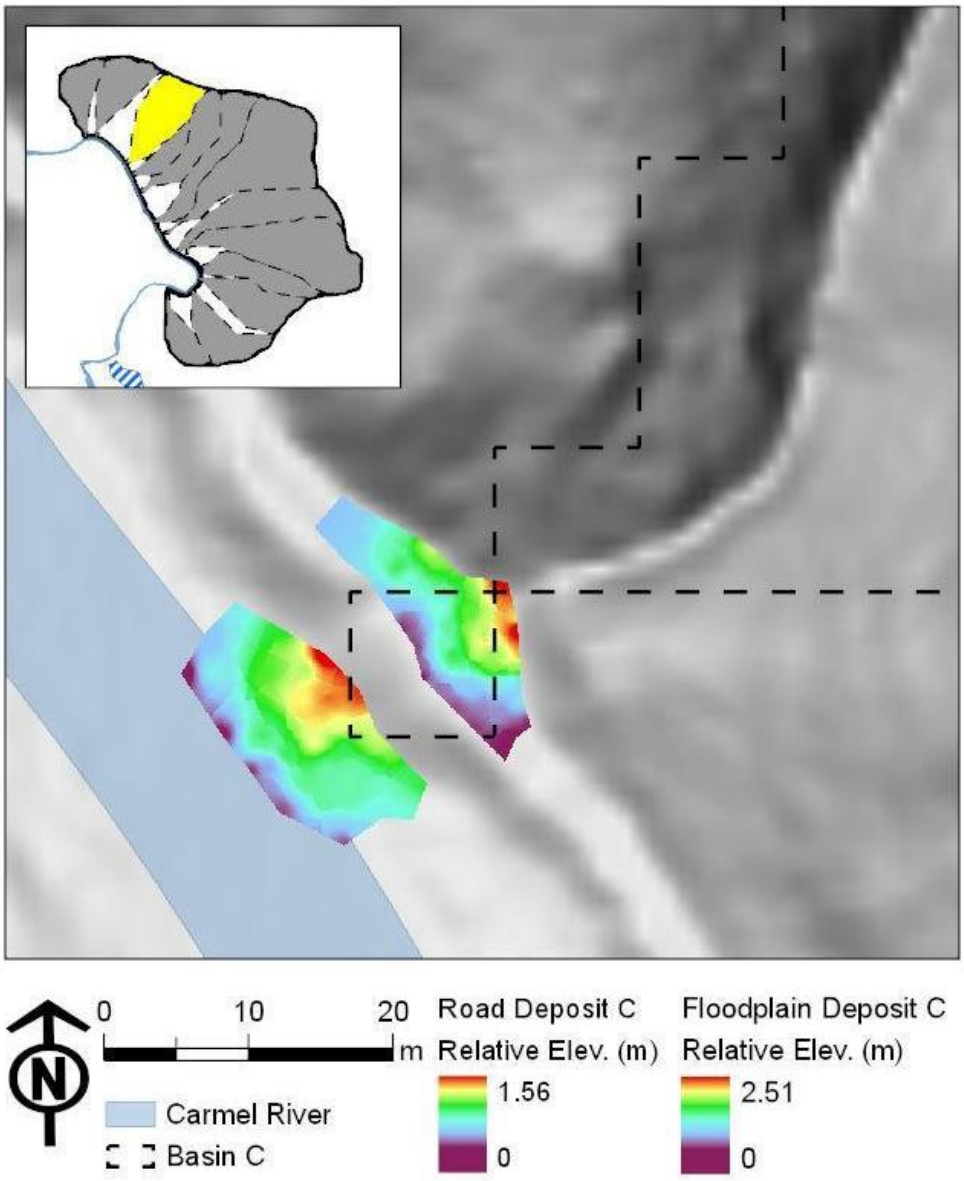
0
10
20
m
N
Carmel River
Basin C
Road Deposit C
Relative Elev. (m)
1.56
0
Floodplain Deposit C
Relative Elev. (m)
2.51
0

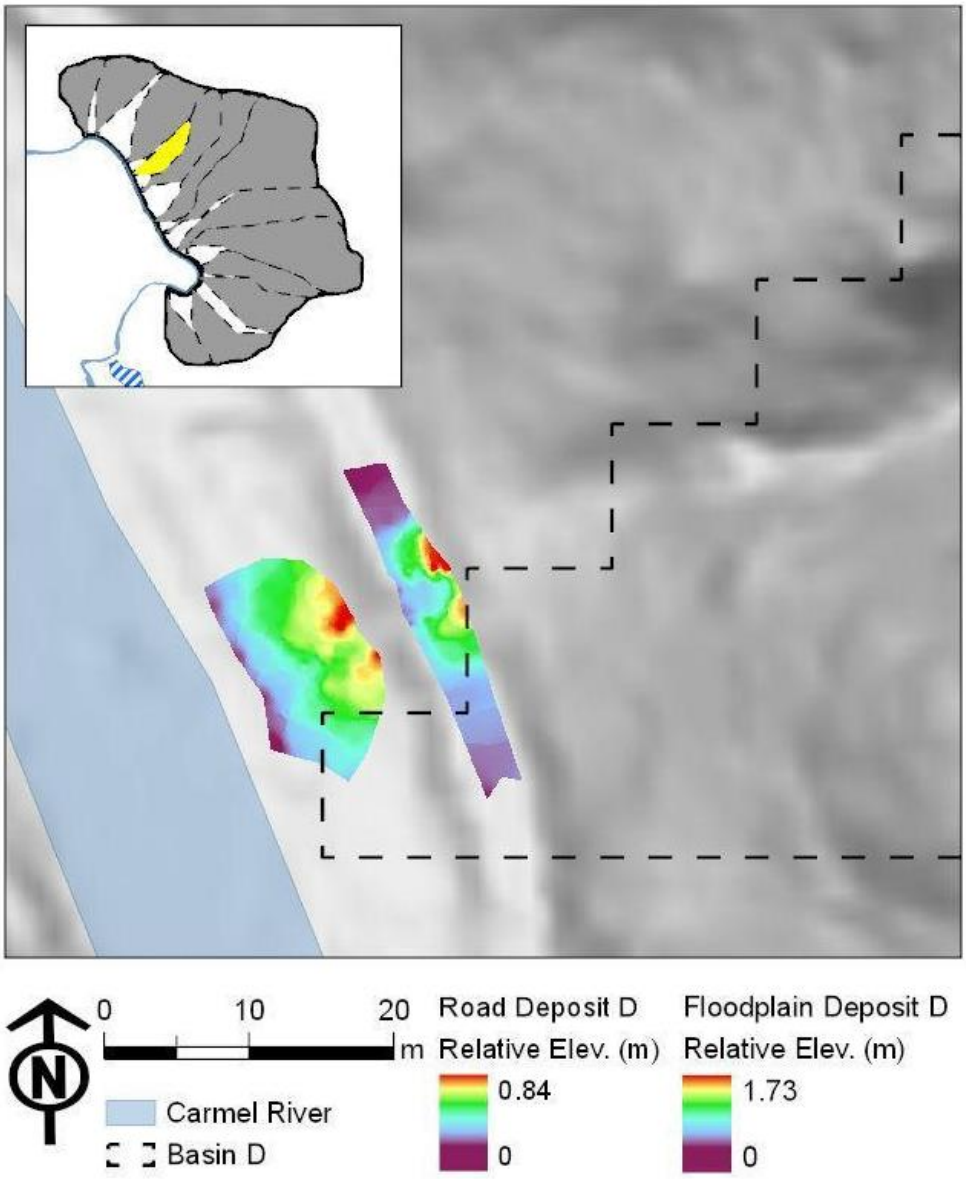
0
10
20
m
N
Carmel River
Basin D
Road Deposit D
Relative Elev. (m)
0.84
0
Floodplain Deposit D
Relative Elev. (m)
1.73
0

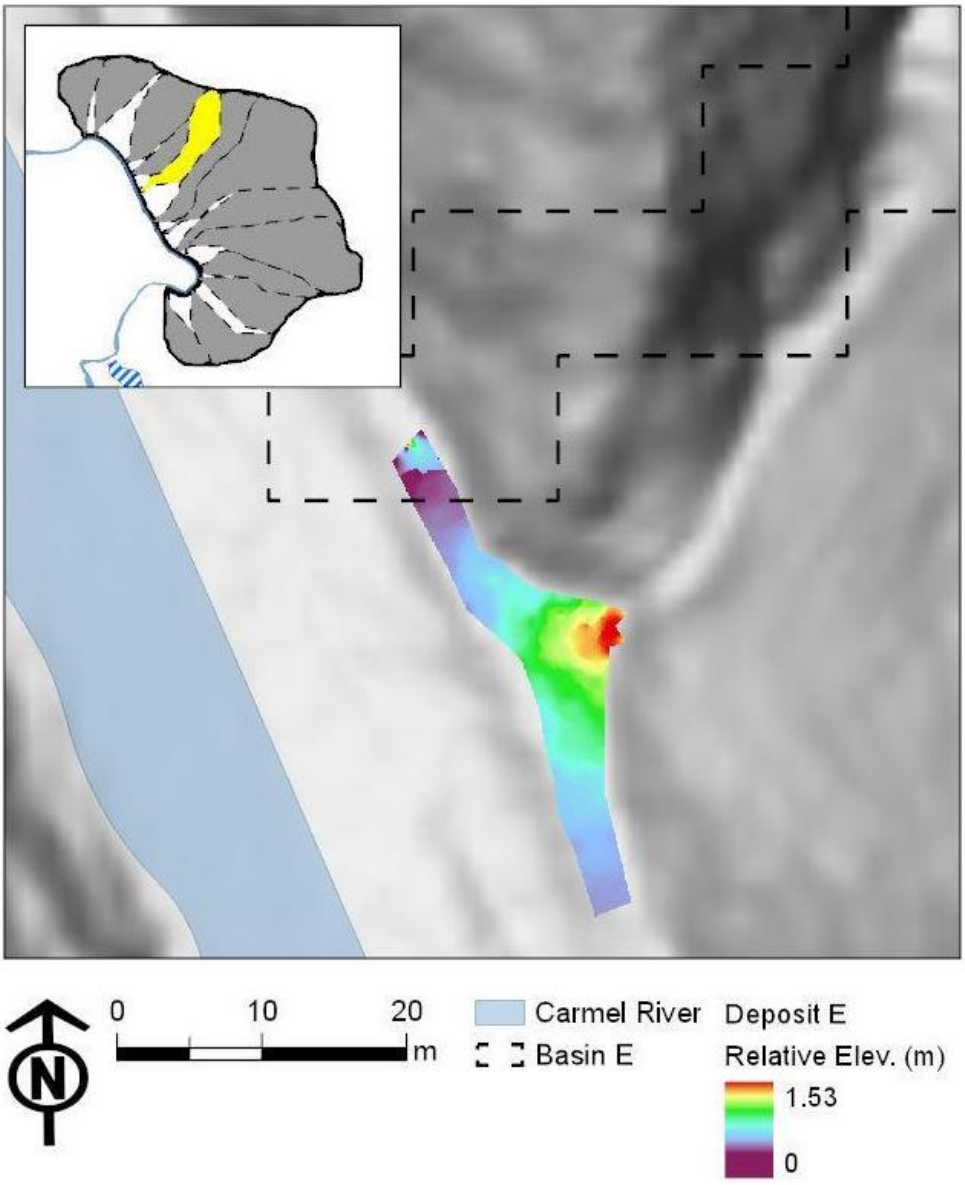
0
10
20
m
Carmel River
Basin E
Deposit E
Relative Elev. (m)
1.53
0

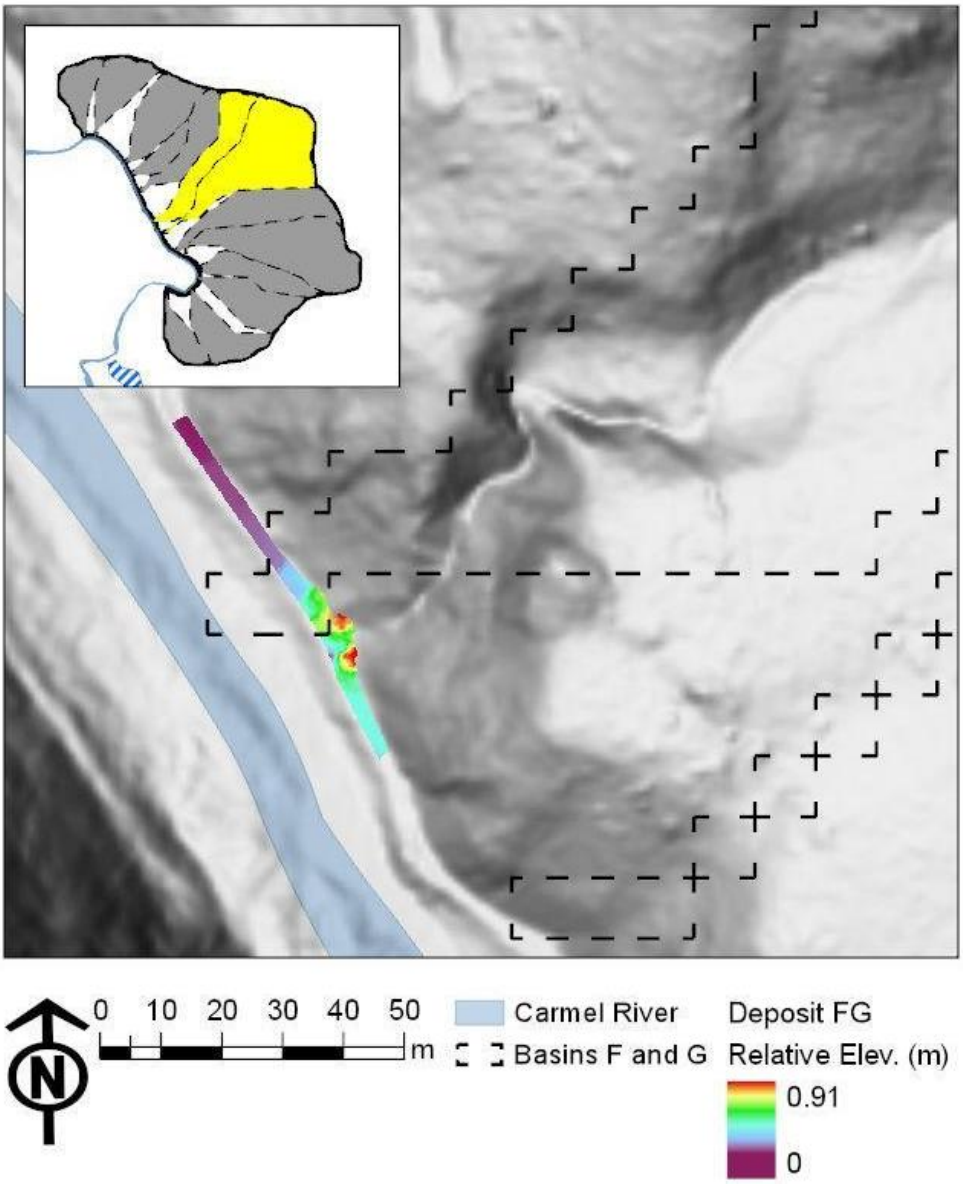
0 10 20 30 40 50
m
N
Carmel River
Basins F and G
Deposit FG
Relative Elev. (m)
0.91
0

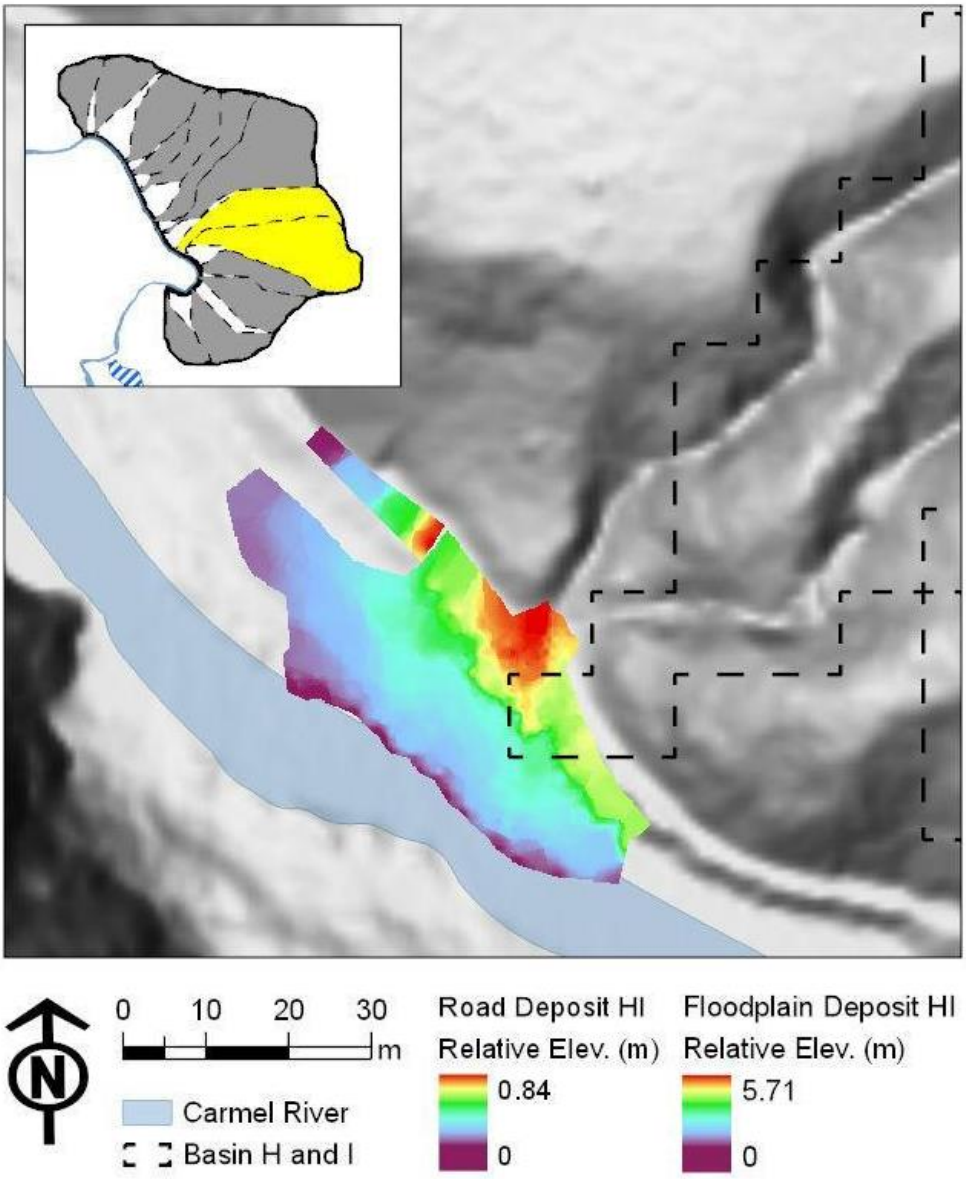
0
10
20
30
m
Carmel River
Basin H and I
Road Deposit HI
Relative Elev. (m)
0.84
0
Floodplain Deposit HI
Relative Elev. (m)
5.71
0

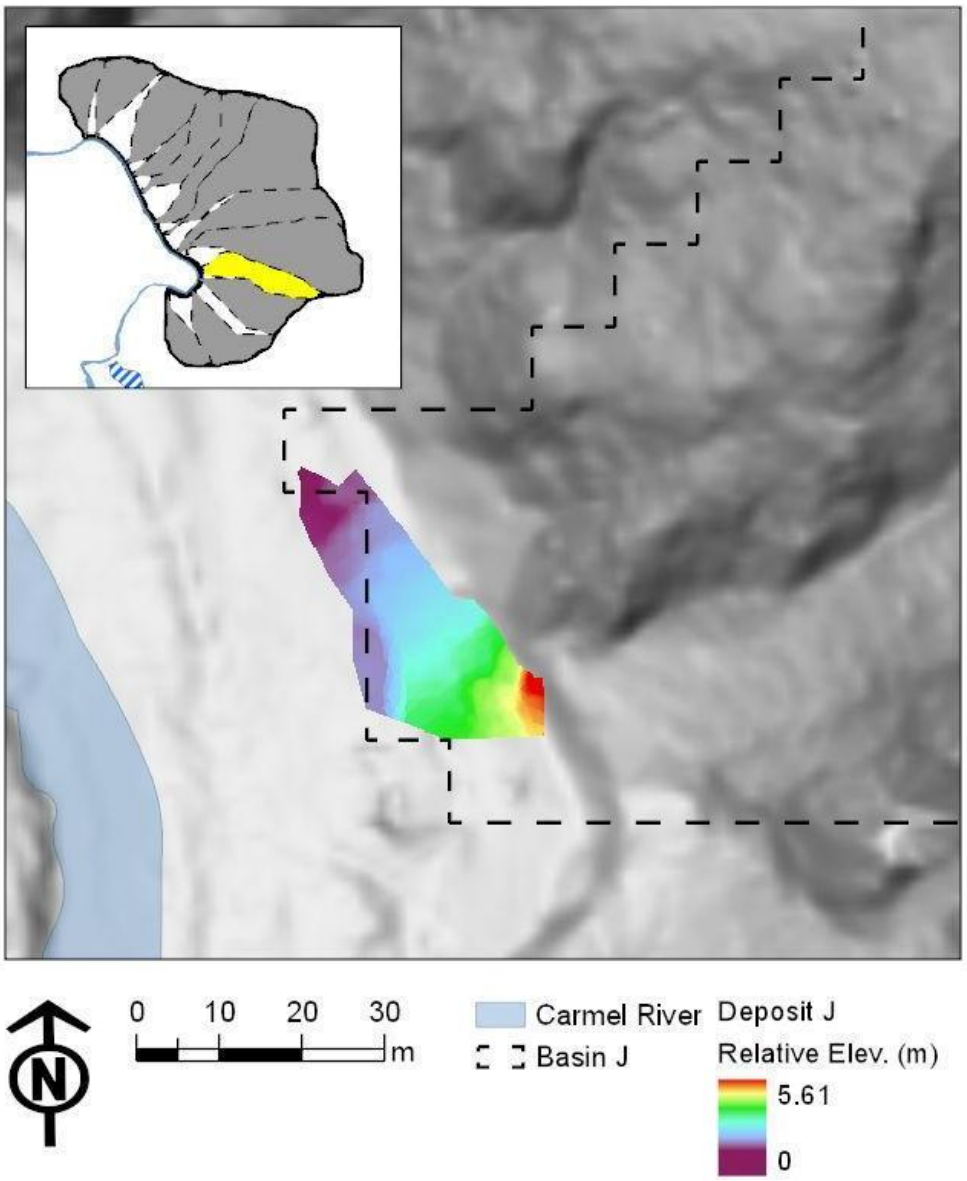
0
10
20
30
m
Carmel River
Basin J
Deposit J
Relative Elev. (m)
5.61
0

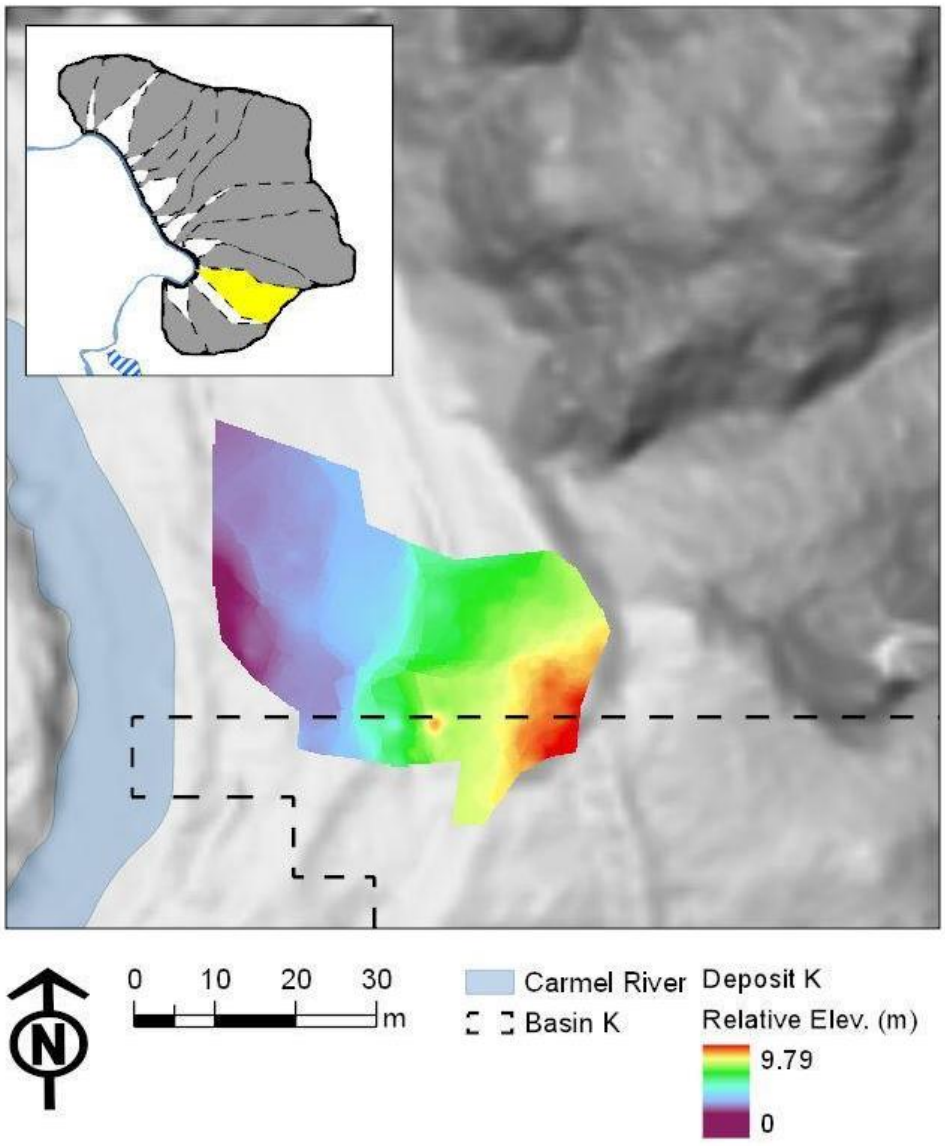
0
10
20
30
m
Carmel River
Basin K
Deposit K
Relative Elev. (m)
9.79
0